A molecular model for carbon black primary particles with internal nanoporosity

Ban, Shuai; Malek, Koroush; Huang, Cheng; Liu, Zhongsheng

Publisher's version / Version de l'éditeur:
https://doi.org/10.1016/j.carbon.2011.04.044
Carbon, 49, 10, pp. 3362-3370, 2011-04-20

CARBON 49 (2011) 3362–3370

available at www.sciencedirect.com

ScienceDirect

journal homepage: www.elsevier.com/locate/carbon

A molecular model for carbon black primary particles with internal nanoporosity

*Shuai Ban, Koroush Malek, Cheng Huang *, Zhongsheng Liu*

National Research Council of Canada, Institute for Fuel Cell Innovation, 4250 Wesbrook Mall, Vancouver, BC, Canada V6T 1W5

ARTICLE INFO

Article history:
Received 27 July 2010
Accepted 15 April 2011
Available online 20 April 2011

ABSTRACT

A molecular model of primary particles of porous carbon black has been developed. Using the hexagonal graphite sheets as building units, we simulated formation of carbon particles consisting of a core–shell structure. Several structural properties of carbon were examined. Graphite layers arrange in a concentric fashion in the shell region near the external surface of carbon. This trend gradually diminishes toward the center of carbon particles, resulting in an amorphous characteristic in the core region. In line with XRD experiments, our simulations show that about half of the graphite sheets in the carbon shell form microcrystalline domains typically consisting of 2–5 layers with a broad interlayer spacing of 0.34–0.4 nm. Starting from nonporous carbon particles with a high density of 2 g/cm^3, a 'digging' approach was further developed to particularly model the internal nanoporosity of mesoporous carbon materials that are often obtained by the silica templating technique. The validity of the modeling technique to generate pores inside carbon particles is discussed in view of reproducing targeted PSDs.

1. Introduction

Carbon black is a type of carbon material with widespread applications such as reinforcing compounds in rubbers [1,2], electrically conductive agents in plastics [3,4], and as catalyst support in proton exchange membrane fuel cells [5,6]. Several types of carbon blacks exist, including furnace black, channel black, lamp black, thermal black and acetylene black [7]. These designations refer to the relevant manufacturing processes which share common procedures; liquid or gaseous hydrocarbons are decomposed at elevated temperature with reduced contents of oxygen [8]. Nowadays, the majority of the worldwide annual production is made through the furnace back process where hydrocarbons are partially combusted and immediately quenched with water [9]. Details of pyrolysis process, carbonization of a parent feedstock, and the formation of porous carbon blacks illustrate the complexity of the reaction conditions, including rates of heating, heat treatment temperature, soak time and ambient gases. During pyrolysis (<700 °C) and carbonization (>700 °C), macromolecular networks start to form from individual carbon precursors. By increasing heat treatment temperature, the thermodynamically unstable network becomes carbonaceous and aromatic as carbon atoms readjust their positions and approximate to the six-membered ring systems that are the building blocks of the graphite-like lamellar constituent molecules. The space elements, generally less than a few nanometers, in between these molecules constitute the microporosity of carbon black. The morphology of resulting micropores depends on the structural details of lamellar constituent molecules that are strongly affected by specific production conditions [10]. Moreover, a wide range of controllable porosity from micro- to macropores can be achieved inside carbon materials by using templating techniques [11,12]. The resulting carbon materials show a regular porous structure, the size of which follows the dimension of templating agents. One of the interesting examples is the

* *Corresponding author:* Fax: +1 604 221 3001.
E-mail address: cheng.huang@nrc-cnrc.gc.ca (C. Huang).
0008-6223/$ - see front matter
doi:10.1016/j.carbon.2011.04.044

mesoporous carbon spheres synthesized by using silica template with the size of a few nanometers [13]. The resulting honeycomb-like carbon framework contains a high volumetric surface area, and the size of mesopores accords well to the diameter of silica templates as evidenced from BET measurement. In particular, the large surface area can always facilitate the applications of templated carbon as catalyst supports and adsorbent agents. Carbon black has different chemical and physical properties from soot and black carbon that is normally generated from incomplete fuel burning [14–17]. In contrast to the low carbon composition (<60%) of soot or black carbon, carbon black material consists mostly of elemental carbon (>97%) in the form of nearly spherical particles of colloidal size less than 100 nm that are further fused together as aggregates in the size of hundreds nanometers. A number of aggregates can interact via van der Waals forces to form a secondary structure known as agglomerates in the scale of micrometers [18,19].

The important properties of carbon black include surface chemistry, surface area, porosity, particle size, microstructure and so on. Many experimental techniques have been employed to characterize these properties of carbon. Early studies used X-ray diffraction (XRD) technique to measure the structural properties of carbon [20–24]. It has been found that the primary carbon particle contains microcrystallites, namely graphite domains. The interlayer spacing, d_{002}, of the microcrystallites can be directly obtained from the [0 0 2] peak, and is used to indicate the graphitization degree in comparison with graphite carbon (d_{002} = 0.335 nm). Based on the [10] band, one was able to calculate the apparent crystalline size in the basal planes with a typical width of 2.5 nm, and present a stacking height strongly depending on carbon types and particle sizes. Later on, efforts have been put to refine the estimation of the crystalline dimensions by combining XRD with Raman spectrum using an empirical formula developed by Tuinstra and Koenig [25]. Systematic characterization studies of a wide range of carbon materials have been performed to examine the validity of Tuinstra and Koenig's method and recommend feasible measurements for carbon characterizations [26,27].

The high resolution transmission electron microscope (HRTEM) has also been used to investigate the carbon structures. In accordance to the HRTEM observation, the individual graphite layer in primary carbon is indeed the basic building unit, instead of graphite crystallites concluded from XRD and Raman measurements [18,19,28,29]. The graphite layers are arrays arranged in a concentric fashion with significant distortion presumably due to the presence of impurities such as oxygen, sulfur, etc. The level of crystalline growth differs from particle to particle, and the stacking variation of poorly developed graphitic layers is responsible for the broad distribution of interlayer spacings measured by XRD. Models of carbon blacks have been proposed by many early studies with a tendency toward the concentric alignment of graphite layers roughly parallel to the external surface of carbon particles [30–32]. This tendency is most pronounced for crystallites located near the carbon surface, and gradually diminishes toward the center of carbon particles.

Based on the knowledge gained from experiments, simulation methods have been widely developed to model and characterize the nanostructures of carbon [33–41]. There are mainly two types of modeling approaches to build structures of nanoporous carbon materials, namely reconstruction methods and mimetic methods. The mimetic approach builds carbon model by mimicking the manufacture process of carbon. Few works have been done in this direction due the complexity of porous carbons and the diversity of processes involved in carbon production. Alternatively, the reconstruction approach is relatively successful in the construction of carbon models that are constrained to satisfy some experimental quantities, including density, interlayer spacing, radial distribution function, porosity, etc. The synthesis procedure of carbon is not considered explicitly. By using build units of carbon at various scales, detailed information of carbon structures can be gained from atomic to mesoscopic level. For instance, Reverse Monte Carlo (RMC) methods were extensively employed to retrace the atomic structures of carbon by comparison with several experimental measurements [34–37]. Beside the basic material properties, e.g. density and the ratio of sp^2/sp^3 carbon hybridization, radial distribution function (RDF) derived from neutron diffraction is the most frequently used quantity to constrain the pair correlation of carbon atoms during simulations. In regards to the porous structures of carbon, RMC is attempted to reproduce the pore size distribution (PSD) obtained from gas physisorption measurements. Agreement between simulation and experiment can be found for the total pore volume, but PSD. The disadvantages of this method are twofold: (1) the simulation domain of carbon particles is limited into a small portion of interiors in the size of a few nanometers. The surface morphology and mesoporous structure of carbon are missed on those scales, even though it is important to consider for carbon used as support materials or adsorbents. (2) The difficulty of simulating the carbon porosity ranging from micro- to mesoscale may hinder further studies such as adsorption phenomenon, mass transport and so on.

In this work, we attempt to model the carbon black primary particles of sizes around 20 nm by using reconstruction approach. The characteristic morphology of carbon black is considered in comparison with XRD and HRTEM measurements. Beside the pair correlation of carbon atoms, the porosity of carbon particles will also be modeled in the range of both micro- (<2 nm) and mesopores (2–50 nm). In particular, our preliminary model of porous carbon black resembles the mesoporous carbon synthesized by using silica templates. It has to be clarified that, in contrast to the mimetic approach, our simulation approach is not designed to model the formation process of carbon black particles. For such a large system, we do not consider stability and structure optimization of porous carbon particles, for which extensive molecular dynamics simulations based on reactive force fields are not evitable [42]. Instead, the characteristic modeling proposed here is to provide a representative carbon model that can facilitate for further simulation studies on extended topics such as carbon-supported catalysts and carbonaceous adsorbent materials.

2. Simulation methods

In our simulation, we adopt the concept that the building unit of carbon black is individual graphite sheets instead of small

graphite crystallites as suggested by HRTEM experiments [19]. The simulated carbon particle thus consists of graphite units with different sizes as shown in Fig. 1. The shape of graphite sheets is chosen as hexagonal, which is energetically the most stable finite two-dimensional structure [43]. In regards to the morphology of carbon particles, two typical regions are distinguished as the amorphous core and the graphitized shell. For convenience, we choose the graphite sheet (core unit) with the diameter $d = 0.7$ nm (consisting of 24 carbon atoms) to construct the amorphous core of all carbon particles. The graphitized shell is built from relatively large graphite sheets (shell unit) with the diameters $d = 2.7$ nm (216 carbon atoms), 3.2 nm (294 carbon atoms), and 3.7 nm (384 carbon atoms), respectively. The intramolecular bonding potentials of flexible carbon sheets were adopted from the work of Walther et al. [44]. The Lennard–Jones parameters for the intermolecular carbon–carbon interaction is taken from GROMACS force field (gmx2.0) with $\sigma = 0.336$ nm, $\varepsilon = 0.0042$ eV. Employing these parameters from various models is acceptable since the force field schemes are identical. Note that the present work does not distinguish between graphite carbon atoms and carbon saturated by other components such as oxygen, nitrogen, hydrogen, etc. This could impact the level of accuracy for the intermolecular interactions of carbon. Also neglecting covalent bonds formed between graphite units on the edges could potentially underestimate the stability of carbon black primary particle [45]. In general, a non-reactive force field is a more effective alternative to simulate C–C bond formation [46]. The C–C bond formation is particularly important to realistically represent the molecular structure of porous particles that are created from non-porous carbon particles. Therefore, the porous particle model that is represented here should not be interpreted as a general molecular model for carbon particles.

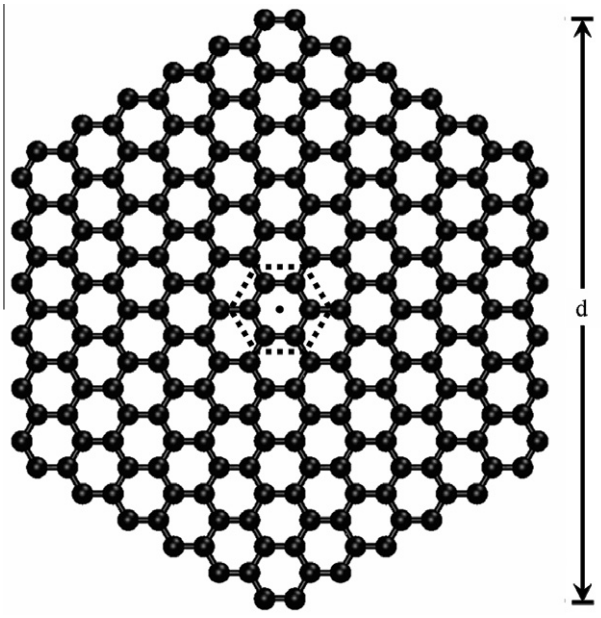

Fig. 1 – Model of the hexagonal graphite unit with $d = 2.7$ nm. The dimension parameter d is defined as the distance from the top to the bottom of the graphite sheet. The dark dot represents the center of the graphite unit. Because of the flexibility, the center of the graphite unit is determined by its central hexagonal ring drawn in dashed circle.

The true density of carbon black is determined by He sorption, which is in the range of 2–2.3 g/cm^3 close to the density of graphite carbon. Such a high density of carbon is the result of the fact that the size of He is tiny enough to enter micropores as small as 0.3 nm. In our simulations, the density of carbon particles is assumed to be 2 g/cm^3. The impact of the porosity on such density is expected to be negligible. Non-equilibrium Molecular Dynamics (MD) simulation is carried out to generate the carbon particles using software Lammps (Large-scale Atomic/Molecular Massively Parallel Simulator) [47]. At the first step, the amorphous core of carbon black is formed by compressing a number of core units into a spherical volume given the density is 2 g/cm^3 inside the cubic simulation box without periodic boundary conditions. The amorphous core with the diameter of 10 nm consists of 2188 core units of diameter $d = 0.7$ nm. An annealing simulation in the range of 300–1000 K is then carried out to randomize the configuration of carbon. Specifically, the system was heated from 300 to 1000 K for 50 ps, and kept at 1000 K for 50 ps, followed by cooling to 300 K for 50 ps, and kept at 300 K for 50 ps. This process is repeated three times. After that, shell units are randomly added to the core surface in a concentric fashion. Similar compression procedure is applied to those shell units, and eventually generates a primary carbon particle with the diameter of 20 nm. During this procedure, core units are kept position restrained. The size of shell units is considered as an important factor impacting the morphology of carbon shells. Given the carbon density of 2 g/cm^3, the selected numbers of shell units are 1704 for $d = 2.7$ nm, 1250 for $d = 3.2$ nm, and 957 for $d = 3.7$ nm, respectively. Thereafter, the final annealing process is performed to equilibrate the whole carbon particle, including both the core and shell units, for 400 ps. In our simulations, this carbon particle is referred as non-porous carbon black due to its high density. Based on the equilibrated carbon particles, structural properties are characterized in terms of RDF, orientation of shell units, crystalline formation, and PSD. The orientation of graphite layers is determined by their central hexagonal rings as shown in Fig. 1. The center of the central hexagonal ring is used to calculate the interlayer spacings of shell units. The algorithm developed by Ban et al. is employed to calculate PSD of carbon particles since this method has already shown the success in characterizing the microporosity of zeolites [48].

Starting from the non-porous carbon particle, a 'digging' approach is developed to generate the pore network inside carbon according to a given PSD, mimicking the pore network inside the silica-templated carbon particles. In this method, interconnected spheres are grown one by one from the surface toward the center of carbon particles. In this way, the good accessibility of porous carbon is obtained. The overlaps of starting pores on carbon surface are minimized. The number and diameters of the pores are adjusted in such way that the targeted PSD can be reproduced. The distance for each growth is equal to $r_{large} + 0.5r_{small}$, where r_{large} is the radius of the larger pore and r_{small} is the radius of smaller one. The

maximum number of pore connectivity is set as six in order to avoid the extensive overlaps. Since there are limited number of experiments which can accurately quantify the PSD in the range of 0.3–1 nm, the targeted PSD is assumed following Gaussian distribution, i.e. $f(x) = ae^{\frac{-(x-b)^2}{2c^2}}$, for the sake of convenience. The parameter a is the height of the PSD curve, b is the mean pore diameter, and c is the factor to control the total volume of 0.5 ml/g for all porous carbon, which is the typical porosity reported in literature. Basically, any type of PSD can be selected to construct porous carbon using the 'digging' method proposed in this work.

3. Results and discussion

3.1. Morphology of carbon black

The widely accepted model of carbon black proposed by Heidenreich et al. is a spherical carbon particle with the concentric organization of small graphite sheets from the surface to the center [32]. The concentric arrangement is more pronounced near the outer surface than the inner cores, leading to the formation of amorphous carbon in the core region. The core–shell structure of carbon black is further supported by

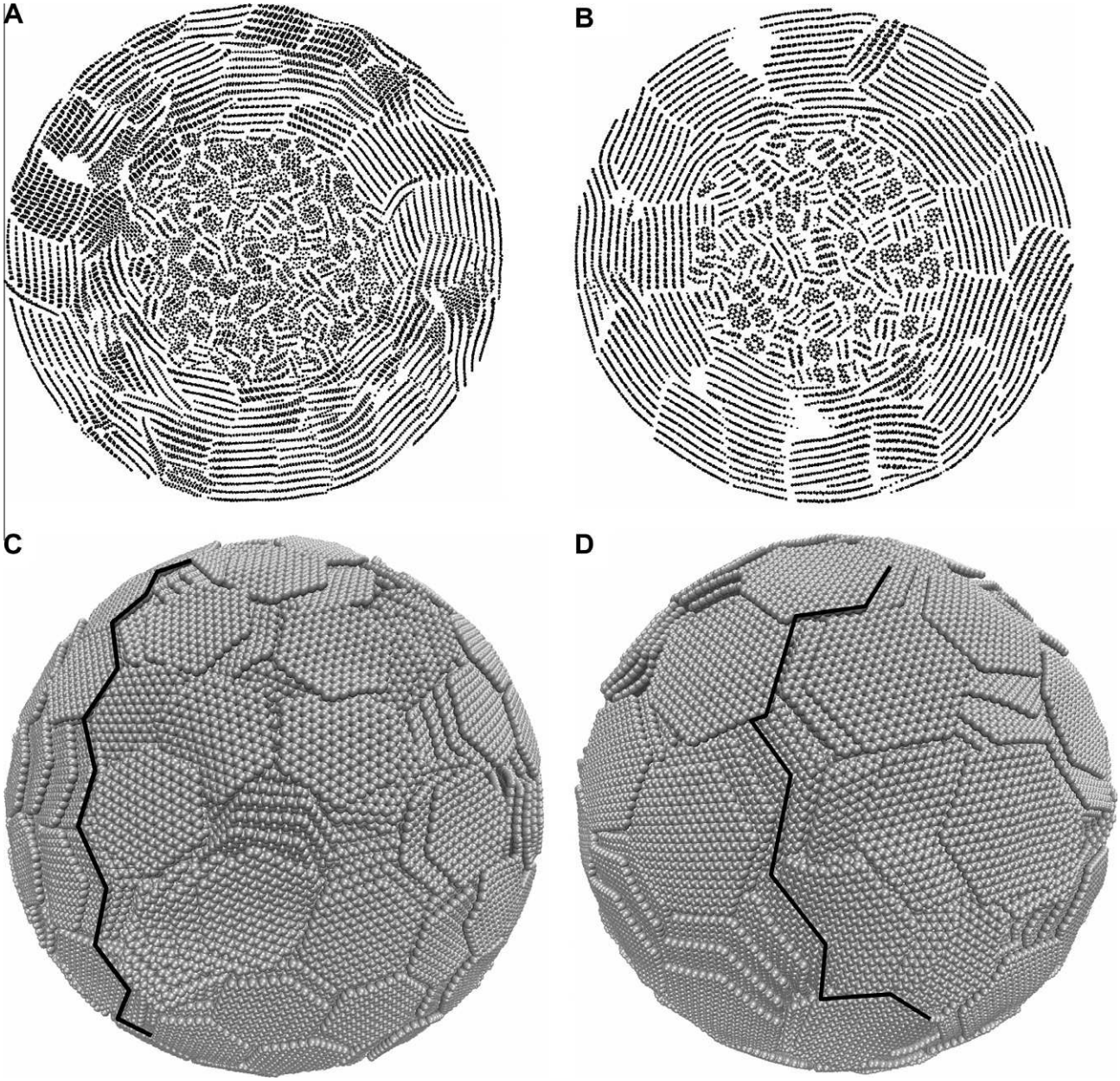

Fig. 2 – Morphology of primary carbon black particles. The slice views are (A) for the carbon particles with shell units d = 2.7 nm, and (B) for the carbon particles with shell units d = 3.7 nm. The snapshots of the surface morphology are (C) for the carbon particles with shell units d = 2.7 nm, and (D) for the carbon particles with shell units d = 3.7 nm. The dark lines are drawn to highlight the grain pattern on the carbon surface. The radii of these carbon black particles are 20 nm, and the densities are 2 g/cm^3.

HRTEM techniques [19]. To examine nanostructures of simulated carbon blacks, slice views of carbon particles are shown in Fig. 2(A and B). Both carbon particles possess the core–shell feature. The core units arrange randomly due to their small sizes. In contrast, the shell units are connected approximately in a concentric fashion, and this tendency is slightly more pronounced for larger shell units Fig. 2(B) than the one in Fig. 2(A). To quantify the orientation of shell units, the angle distributions are calculated for three carbon particles with different shell units in Fig. 3. The core units have a nearly linear angle distribution over the whole range, indicating a random orientation in the core regions. However, the angle distributions of shell units rise rapidly at the small angle range. It reaches a configuration, in which about 70–80% of the shell units faces toward the center of carbon particles with a deviation less than 20°. The larger shell units (d = 3.7 nm) have a well-defined concentric structure compared to that of the small ones (d = 2.7 nm). This effect has also been observed in the experiments, where heat treatment is often applied to partially graphitize carbon blacks [32]. The growth and parallel alignment occurs with graphite layers near the carbon surface, eventually leading to the formation of graphite outer shell [27,49].

Several authors used scanning tunneling microscopy (STM) to investigate the surface morphology of carbon [27,50,51]. The unique feature observed from carbon surfaces has a flake-like arrangement of graphite layers whose edges are characteristic of the growth of aromatic systems. The deposition of these flakes during formation process results in approximately spherical carbon particles. In our simulations, the surface morphology is represented by the external shell units of carbon particles. The snapshots of the surfaces of simulated carbon particles are shown in Fig. 2(C and D). Similar patterns of graphite layers on carbon surfaces are observed in reference to STM experiments [19]. The flake-like morphology of carbon surfaces is rationally reproduced by the hexagonal graphite sheets. Graphite sheets are partially covered with each other, resulting in the surface grain pattern formed by the interconnected flake's edges as illustrated by dark lines in Fig. 2(C and D). This surface property agrees well with the carbon black model developed by Donnet [51]. In addition, the surface roughness is slightly reduced by the graphite sheets with large sizes (3.7 nm) compared to smaller ones (2.7 nm) in Fig. 2(C and D). The grain formation leads to the heterogeneity of the carbon surface by introducing superior adsorption sites for many components such as polymers, metal particles, etc. [51].

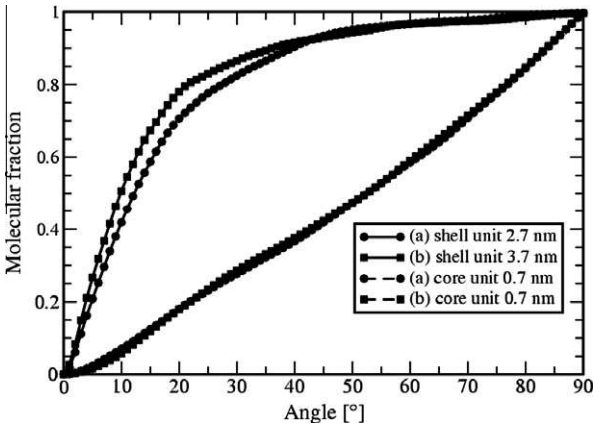

Fig. 3 – The cumulative angle distribution of graphite units in carbon black particles. The sizes of shell units are (a) 2.7 nm and (b) 3.7 nm, respectively. The amorphous cores of both carbon particles consist of identical graphite units with d = 0.7 nm. The molecular fraction is the accumulative number of core/shell units normalized by the total number of core/shell units in carbon particles. The orientation of graphite units is represented by the orientation of their central hexagonal rings with respect to the vector from to its geometry center to the center of the carbon particle. In the case of 0°, the graphite unit is concentric to the carbon surface; the 90° means the graphite unit is perpendicular to the carbon surface.

3.2. *Crystallinity of carbon black*

The RDF profiles derived from X-ray diffraction (XRD) patterns are commonly used to characterize the atomic pair-correlation of carbon blacks. As carbon black contains large number of the graphite units, the major peaks of RDF correspond to the neighboring distance of carbon atoms within the graphite layer. Based on the aromatic structure of graphite with carbon bond length 0.142 nm, the typical distances of carbon atoms are 0.142, 0.246, 0.284, 0.375, 0.425, 0.492, and 0.511 nm, as indicated by crucial peaks shown in Fig. 4(A) [52]. As a general reference, the coordinates of RDF peaks are considered as important quantities rather than the heights that can differ from various carbon samples. In addition to these major peaks, one may note that the base line of RDF rises from about 0.32 nm. This is attributed to the carbon atoms located in different graphite layers since the maximum interlayer spacing of graphite units in carbon blacks is around 0.4 nm [26,32,51]. To explicitly examine the interlayer connectivity of graphite units, the RDF is calculated for only the shell units coordinated by their centers drawn in Fig. 1, instead of single carbon atoms. In Fig. 4(B), the RDF shows a primary peak at the distance of 0.35 nm, which is corresponding to the interlayer spacing of shell units close to the graphite structure. This indicates the organization of small graphite layers in the form of microcrystallites. Even though the building unit used in our simulations is individual graphite sheets, the small crystalline blocks can still be recognized in the form of parallel graphite layers. This behavior is in line with the observation of microcrystalline domains in XRD measurements [26,27]. In particular, the broad RDF peak appearing in the range of 0.4–0.5 nm suggests that the graphite layers are more loosely bonded to each other than graphite-type carbons, corresponding to the wide distribution of interlayer spacings derived from XRD experiments. Our simulations show that the building unit in carbon blacks is indeed the individual graphite sheet as seen from HRTEM. Those graphite sheets are interconnected with each other, forming microcrystallites as derived from XRD. The interlayer distances of graphite units are ranging from 0.35 to 0.5 nm, resulting in a less well-defined crystalline structure than graphite carbons.

The size distribution of graphite microcrystallites in carbon particles is plotted in Fig. 5. The threshold of crystalline

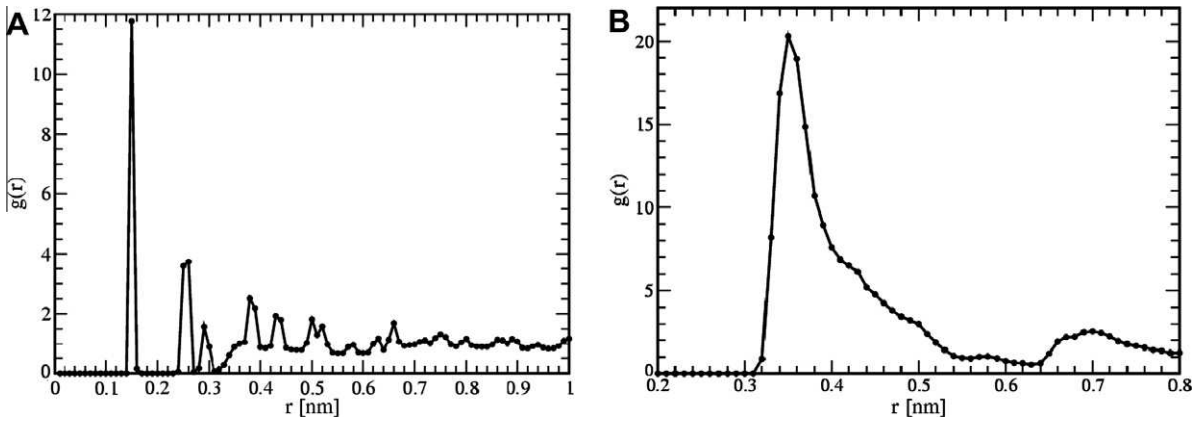

Fig. 4 – The radial distribution function (RDF) of (A) all carbon atoms and (B) the centers of shell units in the carbon black particle formed by core units d = 0.7 nm and shell units d = 2.7 nm.

interlayer spacing is set at 0.4 nm according to the largest distance derived from XRD [26,32]. The simulation results show that about 50% of the graphite layers are those do not belong to any microcrystallite. The other 50% graphite units form microcrystallites containing mainly 2–5 graphite layers. This trend is minor dependent on the sizes of shell units. The calculated crystalline sizes agree with experimental data obtained from XRD and Raman spectra, where the sizes of graphite layers are 2–4 nm and the heights of crystallites are 1.1–2.0 nm corresponding to 3–6 parallel layers [18,26,32,51–53].

3.3. *Porosity of carbon black*

The porosity of carbon black particles is characterized by PSD shown in Fig. 6. As expected, the high density of carbon particles results in negligible microporosity. All three carbon samples with different sizes of shell units have the total pore volumes less than 0.03 ml/g. Compared to the Vulcan black known as the non-porous carbon, the pore volume measured by N_2 physisorption is about 0.05 ml/g, close to the value obtained from our carbon models [5,54]. We refer to this type of carbon black as non-porous carbon black in our simulations. These carbons are believed to be quite inaccessible for large adsorbates due to the lack of permeation paths. The total pore volume increases with the size of shell units, leading to the sequence of 0.021 ml/g for d = 2.7 nm, 0.025 ml/g for d = 3.2 nm, and 0.027 ml/g for d = 3.7 nm. This tendency is attributed to the fact that a random packing of larger graphitic units may lead to a higher free volume of interlayer gaps than smaller ones. Accordingly, the accurate density of carbon blacks with various shell units can be corrected as 2.09 g/cm^3 for d = 2.7 nm, 2.11 g/cm^3 for d = 3.2 and 3.7 nm.

Starting from the non-porous carbon particles, the 'digging' procedure is used to generate internal porosity, following the targeted PSD with Gaussian distribution, which mimics the silica templating process. One should notice that in our study, our porous carbon model particularly primarily mimics templating approach, and thus can not be referred to as a general molecular model for porous carbon nanoparticles. Moreover, the carbon frameworks are kept rigid and not

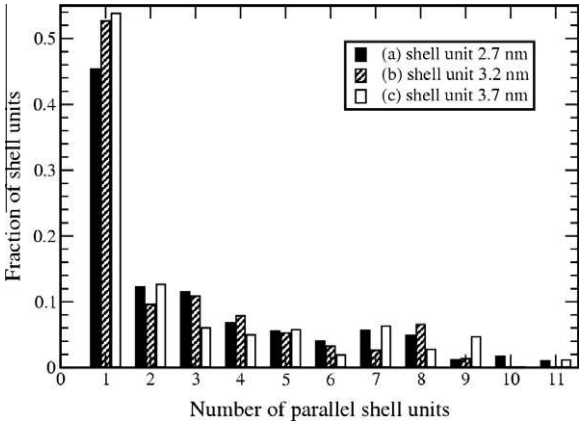

Fig. 5 – The size distribution of the graphite microcrystallites in carbon black particles. The microcrystallite consists of parallel shell units with interlayer spacings smaller than 0.4 nm. The interlayer spacing is calculated from the centers of shell units as shown in Fig. 1.

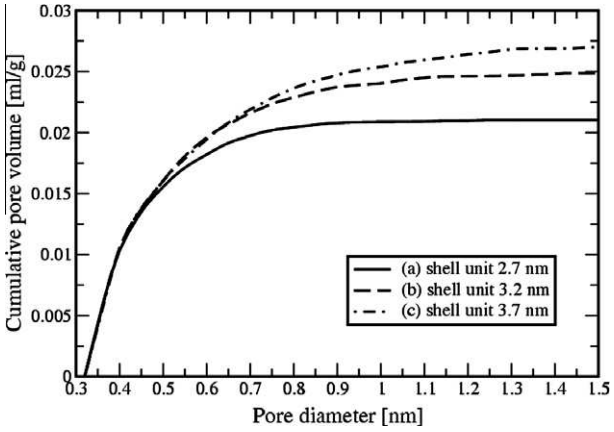

Fig. 6 – The cumulative pore volume of carbon black particles formed by core units d = 0.7 nm and shell units with (a) d = 2.7 nm, (b) d = 3.2 nm, and (c) d = 3.7 nm, respectively. The total pore volumes are (a) 0.021 ml/g, (b) 0.025 ml/g, and (c) 0.027 ml/g.

optimized in a dynamic manner. This treatment is acceptable to certain extent as silica-templated carbon particles were experimentally found having the stable honeycomb-like structures under ambient conditions. When comparing with experimental PSD, one needs to note that beyond the micropore regime, e.g. 2 nm, the total porosity can be contributed from pores located either inside carbon particles or between primary carbon particles. In our case, only porosity within carbon particles is considered. Using carbon particles with different shell units, various porosities are generated and the corresponding PSD is shown in Fig. 7(A). As expected, the calculated PSD is independent on the shell units chosen for constructing carbon particles. The PSD of all three carbon samples matches well with the targeted PSD except for the pores smaller than 1 nm. A close inspection of carbon snapshots reveals that the existence of micropores (<1 nm) is attributed to the irregularity of the pore system. Such a phenomenon is also evidenced from the BET measurement of mesoporous carbon, where a noticeable amount of micropores appears in addition to the artificially created mesopores [13]. The total pore volumes of all three carbon samples are 0.54 ml/g. Based on initial micropore volumes of starting car-

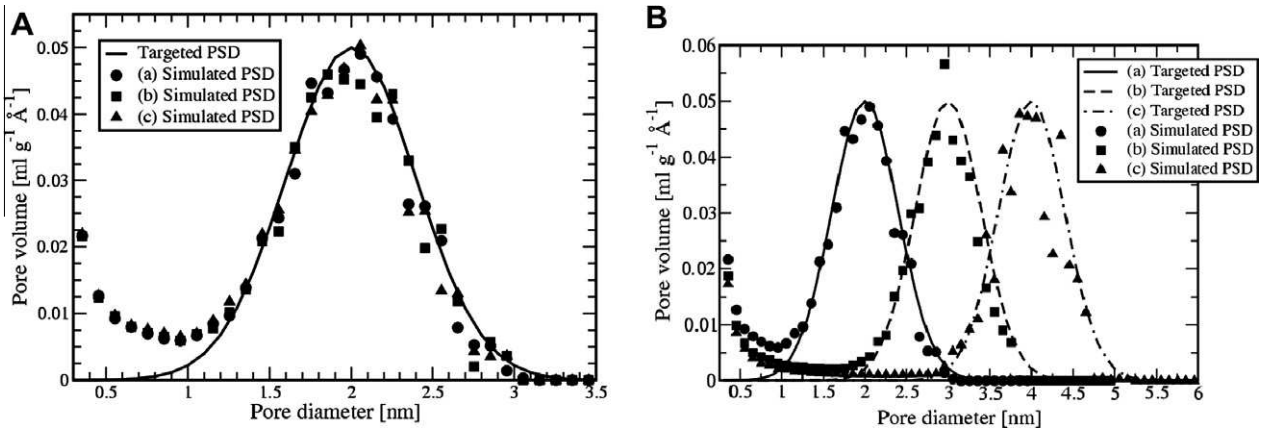

Fig. 7 – The pore size distributions of carbon black particles. (A) The carbon particles are formed by core units d = 0.7 nm and shell units (a) d = 2.7 nm, (b) d = 3.2 nm, and (c) d = 3.7 nm, respectively. The targeted pore size distribution follows the Gaussian distribution $f(x) = ae^{-\frac{(x-b)^2}{2c^2}}$ with a = 0.05, b = 20, and c = 3.99, having a total pore volume = 0.5 ml/g. The total pore volumes of all three carbon samples are 0.54 ml/g. (B) The carbon particles are formed by core units d = 0.7 nm and shell units d = 2.7 nm. The targeted pore size distributions follow the Gaussian distribution $f(x) = ae^{-\frac{(x-b)^2}{2c^2}}$ with a = 0.05, c = 3.99, (a) b = 20, (b) b = 30, and (c) b = 40, all having a total pore volume = 0.5 ml/g. The total pore volumes of carbon samples are (a) 0.54, (b) 0.51, and (c) 0.5 ml/g.

Fig. 8 – Slice views of porous carbon black particles. The porosity of carbon particles is generated according to the targeted pore size distributions $f(x) = ae^{-\frac{(x-b)^2}{2c^2}}$ with a = 0.05, c = 3.99, and (A) b = 20, (B) b = 40. The total pore volumes of carbon samples are (A) 0.54 ml/g and (B) 0.5 ml/g.

bon particles, the corrected pore volume is about 0.52 ml/g, in well agreement with the target volume of 0.5 ml/g. Targeted PSD with various mean pore sizes is used to generate porous carbons, and the results is shown in Fig. 7(B). Basically, all three targeted PSDs can be reproduced by our carbon models. The total pore volumes are 0.54 ml/g for d_{mean} = 20 nm, 0.51 ml/g for d_{mean} = 30 nm, and 0.5 ml/g for d_{mean} = 40 nm, respectively. A visual inspection reveals that the marching quality of PSD is gradually reduced along the mean pore diameter. This is due to the size of our carbon particles, namely 20 nm, which is not sufficient for the growth of pores as large as 4 nm. The slice views of porous carbon in Fig. 8 visualize pore networks generated inside carbon particles. The interconnected pores form channel-like structures, running from the surface to the center of carbon particles. One way to verify the porous structure of carbon black is the simulation, e.g. grand-canonical Monte Carlo methods, of gas adsorption isotherms that are commonly deployed to validate molecular models of nanomaterials. These resulting carbon particles possess high accessibility and are very suitable molecular models for the further simulation studies of carbon-supported catalysts and carbonaceous diffusion and separation media.

4. Conclusion

A molecular model of carbon black has been developed in order to gain deep understanding of carbon nanostructures on an atomistic level. Using hexagonal graphite sheets as building units, the carbon particles containing amorphous cores and crystalline shells were generated. The graphite units near the surface of carbon particles orientated in a concentric fashion. The trend gradually disappears towards the center of carbon black. These structural properties agree with many carbon models proposed by early works. The visualization of simulated carbon surfaces reveals that the continuous grain pattern is formed by the joint edges of graphite layers. Evidenced from the reinforcing effect of carbon blacks on rubbers, the continuous grains, in addition to other chemical and structural defects, on the carbon surface are believed to be the superior adsorption sites for long chain molecules.

The pair-correlations of carbon atoms in simulated carbon particles show consistent neighboring distances with graphite carbons. This tendency is attributed to the graphite units used to build the carbon particles. Although the individual graphite sheets are the building units for constructing carbon particles, the graphite microcrystallites are still evident, especially near the surface of carbons. Microcrystallites are formed primarily by the interlayer bonding of graphite units within the distances of 0.34–0.4 nm. About 50% of the graphite units near the carbon surface are involved in the crystallites. This finding illustrates the crystalline structure of carbon blacks that has been under debate between XRD and HRTEM experiments for decades.

The carbon particles are generated with the high density, i.e. 2 g/cm^3, resulting in the existence of negligible micropore volume 0.02–0.03 ml/g. The larger sizes of graphite units hinder the packing efficiency and lead to higher micropore volume. Given the Gaussian-type PSD as targets, the created porosity of carbon particles is able to reproduce the targeted PSD with a good quality. The micropores smaller than 1 nm are always present in carbon particles, and generating porosity in this range requires the accurate analysis of experimental measurements in the subnano scale. For nanopores, the sizes of simulated carbon particles also need to be sufficiently large in order to obtain a good statistical sampling. The pore network of our carbon models possesses a high accessibility due to the channel structure running from the surface to the center of carbon particles. This feature provides modeling opportunities to further study the carbon-related phenomena such as water and gas transport and adsorption in carbon-supported catalysts in polymer electrolyte fuel cell, as well in carbonaceous diffusion and separation media.

REFERENCES

[1] Rigbi Z. Reinforcement of rubber by carbon black. Berlin/Heidelberg: Springer; 1980. p. 21–68.
[2] Kohls DJ, Beaucage G. Rational design of reinforced rubber. Curr Opinion Solid State Mater Sci 2002;6(3):183–94.
[3] Baltá Calleja FJ, Bayer RK, Ezquerra TA. Electrical conductivity of polyethylene–carbon-fibre composites mixed with carbon black. J Mater Sci 1988;23(4):1411–5.
[4] Balberg I. Tunneling and nonuniversal conductivity in composite materials. Phys Rev Lett 1987;59(12):1305–8.
[5] Soboleva T, Zhao XS, Malek K, Xie Z, Navessin T, Holdcroft S. On the micro-, meso-, and macroporous structures of polymer electrolyte membrane fuel cell catalyst layers. ACS Appl Mater Interfaces 2010;2(2):375–84.
[6] Guha A, Lu WJ, Zawodzinski J, Schiraldi DA. Surface-modified carbons as platinum catalyst support for PEM fuel cells. Carbon 2007;45(7):1506–17.
[7] Wissler M. Graphite and carbon powders for electrochemical applications. J Power Sources 2006;156(2):142–50.
[8] Donnet JB, Bansal RC, Wang MJ. Carbon black: science and technology. 2nd ed. New York: Marcel Dekker Inc.; 1993.
[9] Rothbuhr L, Witte J. Process for the production of furnace black. US patent 4292291, 1979.
[10] Patrick JW. Porosity in carbons: characterization and applications. London: Edward Arnold; 1995.
[11] Lee J, Kim J, Hyeon T. Recent progress in the synthesis of porous carbon materials. Adv Mater 2006;18(16):2073–94.
[12] Lu A, Schüth F. Nanocasting: a versatile strategy for creating nanostructured porous materials. Adv Mater 2006;18(14):1793–805.
[13] Liu H, Zheng S, Zhang J, Zhang L, Zhang J. Ultrasonic spray pyrolyzed iron–polypyrrole mesoporous spheres for fuel cell oxygen reduction electrocatalysts. J Mater Chem 2009;19(4):468–70.
[14] Popovitcheva OB, Persiantseva NM, Trukhin ME, Trukhin GB, Shonija NK, Buriko YY, et al. Experimental characterization of aircraft combustor soot: microstructure, surface area, porosity and water adsorption. Phys Chem Chem Phys 2000;2(19):4421–6.
[15] Popovicheva OB, Persiantseva NM, Kuznetsov BV, Rakhmanova TA, Shonija NK, Suzanne J, et al. Microstructure and water adsorbability of aircraft combustor soots and kerosene flame soots: toward an aircraft-generated soot laboratory surrogate. J Phys Chem A 2003;107(47):10046–54.
[16] Demirdjian B, Ferry D, Suzanne J, Popovicheva OB, Persiantseva NM, Shonija NK. Heterogeneities in the

microstructure and composition of aircraft engine combustor soot: impact on the water uptake. J Atmos Chem 2007;56(1):83–103.
[17] Popovicheva O, Persiantseva NM, Shonija NK, DeMott P, Koehler K, Petters M, et al. Water interaction with hydrophobic and hydrophilic soot particles. Phys Chem Chem Phys 2008;10(17):2332–44.
[18] Zhu WZ, Miser DE, Geoffrey CW, Hajaligol MR. HRTEM investigation of some commercially available furnace carbon blacks. Carbon 2004;42(8–9):1841–5.
[19] Ávila-Brande D, Katcho NA, Urones-Garrote E, Gómez-Herrero A, Landa-Cánovas AR, Otero-Díaz LC. Nano-structured carbon obtained by chlorination of NbC. Carbon 2006;44(4):753–61.
[20] Biscoe J, Warren BE. An X-ray study of carbon black. J Appl Phys 1942;13(6):364–71.
[21] Warren BE. X-ray diffraction study of carbon black. J Chem Phys 1934;2(9):551–5.
[22] Alexander L, Darin SR. X-ray diffraction study of four reinforcing carbon blacks. J Chem Phys 1955;23(3):594–5.
[23] Alexander LE, Sommer EC. Systematic analysis of carbon black structures. J Phys Chem 1956;60(12):1646–9.
[24] Austin AE, Hedden WA. Graphitization processes in cokes and carbon blacks. Ind Eng Chem 1954;46(7):1520–4.
[25] Tuinstra F, Koenig JL. Raman spectrum of graphite. J Chem Phys 1970;53(3):1126–30.
[26] Cuesta A, Dhamelincourt P, Laureyns J, Martínez-Alonso A, Tascón JMD. Comparative performance of X-ray diffraction and Raman microprobe techniques for the study of carbon materials. J Mater Chem 1998;8(12):2875–9.
[27] Cancado LG, Takai K, Enoki T, Endo M, Kim YA, Mizusaki H, et al. General equation for the determination of the crystallite size L_a of nanographite by Raman spectroscopy. Appl Phys Lett 2006;88(16):163106–8.
[28] Harris PJF. Imaging the atomic structure of activated-carbon. J Phys Condens Matter 2008;20(36):362201–5.
[29] Harris PJF. New perspectives on the structure of graphitic carbons. Crit Rev Solid State Mater Sci 2005;30(4):235–53.
[30] Heckman FA, Harling DF. Progressive oxidation of selected particles of carbon black: further evidence for a new microstructural model. Rubber Chem Technol 1966;39(1):1–13.
[31] Donnet JB, Schultz J, Eckhardt A. Etude de la microstructure d'un noir de carbone thermique. Carbon 1968;6(6):781–6.
[32] Heidenreich RD, Hess WM, Ban LL. A test object and criteria for high resolution electron microscopy. J Appl Crystallogr 1968;1(1):1–19.
[33] Moulin F, Picaud S, Hoang PNM, Jedlovszky P. Grand canonical Monte Carlo simulation of the adsorption isotherms of water molecules on model soot particles. J Chem Phys 2007;127(16). 164719-1–11.
[34] Thomson KT, Gubbins KE. Modeling structural morphology of microporous carbons by reverse Monte Carlo. Langmuir 2000;16(13):5761–73.
[35] Nguyen TX, Cohaut N, Bae JS, Bhatia SK. New method for atomistic modeling of the microstructure of activated carbons using hybrid reverse Monte Carlo simulation. Langmuir 2008;24(15):7912–22.
[36] Katcho NA, Zetterström P, Lomba E, Marco JF, Urones-Garrote E, Ávila-Brande D, et al. Structure of carbon nanospheres prepared by chlorination of cobaltocene: experiment and modeling. Phys Rev B 2008;77(19):195402–12.
[37] Zetterström P, Urbonaite S, Lindberg F, Delaplane RG, Leis J, Svensson G. Reverse Monte Carlo studies of nanoporous carbon from TiC. J Phys Condens Matter 2005;17(23):3509–24.
[38] Terzyk AP, Furmaniak S, Gauden PA, Harris PJF, Wloch J. Testing isotherm models and recovering empirical relationships for adsorption in microporous carbons using virtual carbon models and grand canonical Monte Carlo simulations. J Phys Condens Matter 2008;20(38). 385212-1–15.
[39] Bandosz TJ, Biggs MJ, Gubbins KE, Hattori Y, Iiyama T, Kaneko K, et al. Molecular models of porous carbons. Chem Phys Carbon 2003;28:41–228.
[40] Biggs MJ, Buts A. Virtual porous carbons: what they are and what they can be used for. Mol Simul 2006;32(7):579–93.
[41] Powles RC, Marks NA, Lau DWM. Self-assembly of sp^2-bonded carbon nanostructure from amorphous precursors. Phys Rev B 2009;79(7). 075430-1–11.
[42] Hantal G, Picaud S, Hoang PNM, Voloshin VP, Medvedev NN, Jedlovszky P. Water adsorption isotherms on porous onionlike carbonaceous particles. Simulations with the grand canonical Monte Carlo method. J Chem Phys 2010;133(14). 144702-1–12.
[43] Robertson J, O'Reilly EP. Electronic and atomic structure of amorphous carbon. Phys Rev B 1987;35(6):2946–57.
[44] Walther JH, Jaffe R, Halicioglu T, Koumoutsakos P. Carbon nanotubes in water: structural characteristics and energetics. J Phys Chem B 2001;105(41):9980–7.
[45] Donnet JB, Custodero E. Ordered structures observed by scanning tunnelling microscopy at atomic scale on carbon black surfaces. Carbon 1992;30(5):813–7.
[46] Cheung S, Deng W, van Duin ACT, Goddard WA. $ReaxFF_{MgH}$ reactive force field for magnesium hydride systems. J Phys Chem A 2005;109(5):851–9.
[47] Plimpton S. Fast parallel algorithms for short-range molecular dynamics. J Comput Phys 1995;117(1):1–19.
[48] Ban S, Vlugt TJH. Zeolite microporosity studied by molecular simulation. Mol Simul 2009;35(12):1105–15.
[49] Gruver GA. The corrosion of carbon black in phosphoric acid. J Electrochem Soc 1978;125(10):1719–20.
[50] Donnet JB, Custodero E. Ordered structures observed by scanning tunnelling microscopy at atomic scale on carbon black surfaces. Carbon 1992;30(5):813–5.
[51] Donnet JB. Fifty years of research and progress on carbon black. Carbon 1994;32(7):1305–10.
[52] Darmstadt H, Roy C, Kaliaguine S, Xu GY, Auger M, Tuel A, et al. Solid state ^{13}C NMR spectroscopy and XRD studies of commercial and pyrolytic carbon blacks. Carbon 2000;38(9):1279–87.
[53] Kamegawa K, Nishikubo K, Yoshida H. Oxidative degradation of carbon blacks with nitric acid (I) – changes in pore and crystallographic structures. Carbon 1998;36(4):433–41.
[54] Stoeckli F, Guillot A, Slasli AM, Hugi-Cleary D. Microporosity in carbon blacks. Carbon 2002;40(2):211–5.